The millimeter-wave spectrum of the SiP radical ($X^2\Pi_i$): Rotational perturbations and hyperfine structure

Cite as: J. Chem. Phys. **157**, 184307 (2022); https://doi.org/10.1063/5.0118939 Submitted: 06 August 2022 • Accepted: 06 October 2022 • Published Online: 10 November 2022









ARTICLES YOU MAY BE INTERESTED IN

Electronic excitation spectra of jet-cooled phenyl isocyanate, m-tolyl isocyanate, and p-phenylene diisocyanate: Assignment of the cis and trans rotational isomers

The Journal of Chemical Physics 157, 184305 (2022); https://doi.org/10.1063/5.0107088

Understanding electronic structures, chemical bonding, and fluxional behavior of $Lu_2@C_{2n}$ (2n = 76-88) by a theoretical study

The Journal of Chemical Physics 157, 184306 (2022); https://doi.org/10.1063/5.0100652

Noise and thermodynamic uncertainty relation in "underwater" molecular junctions
The Journal of Chemical Physics 157, 184304 (2022); https://doi.org/10.1063/5.0125086





The millimeter-wave spectrum of the SiP radical ($X^2\Pi_i$): Rotational perturbations and hyperfine structure

Cite as: J. Chem. Phys. 157, 184307 (2022); doi: 10.1063/5.0118939 Submitted: 6 August 2022 • Accepted: 6 October 2022 • **Published Online: 10 November 2022**











M. A. Burton, 1,a) D P. M. Sheridan, 2 D and L. M. Ziurys 1,3 D



AFFILIATIONS

- Department of Chemistry and Biochemistry, University of Arizona, 1305 E 4th Street, Tucson, Arizona 85719, USA
- ² Department of Chemistry and Biochemistry, Canisius College, 2001 Main St., Buffalo, New York 14208, USA
- Department of Astronomy, Steward Observatory, University of Arizona, 944 N Cherry Ave., Tucson, Arizona 85718, USA

ABSTRACT

The millimeter/submillimeter-wave spectrum of the SiP radical $(X^2\Pi_i)$ has been recorded using direct absorption spectroscopy in the frequency range of 151-532 GHz. SiP was synthesized in an AC discharge from the reaction of SiH₄ and gas-phase phosphorus, in argon carrier gas. Both spin-orbit ladders were observed. Fifteen rotational transitions were measured originating in the Ω = 3/2 ladder, and twelve in the $\Omega = 1/2$ substate, each exhibiting lambda doubling and, at lower frequencies, hyperfine interactions from the phosphorus nuclear spin of I = 1/2. The lambda-doublets in the $\Omega = 1/2$ levels appeared to be perturbed at higher J, with the f component deviating from the predicted pattern, likely due to interactions with the nearby excited $A^2\Sigma^+$ electronic state, where $\Delta E_{\Pi,\Sigma} \sim 430 \text{ cm}^{-1}$. The data were analyzed using a Hund's case a_{β} Hamiltonian and rotational, spin-orbit, lambda-doubling, and hyperfine parameters were determined. A $^{2}\Pi/^{2}\Sigma$ deperturbation analysis was also performed, considering spin-orbit, spin-electronic, and L-uncoupling interactions. Although SiP is clearly not a hydride, the deperturbed parameters derived suggest that the pure precession hypothesis may be useful in assessing the ${}^2\Pi / {}^2\Sigma$ interaction. Interpretation of the Fermi contact term, b_F , the spin-dipolar constant, c, and the nuclear spin-orbital parameter, a, indicates that the orbital of the unpaired electron is chiefly p_{π} in character. The bond length in the v = 0 level was found to be $r_0 = 2.076$ Å, suggestive of a double bond between the silicon and phosphorus atoms.

Published under an exclusive license by AIP Publishing. https://doi.org/10.1063/5.0118939

I. INTRODUCTION

Molecules and materials containing the Si-P bond have attracted much interest recently in the chemical, physics, and engineering communities. Silicon phosphide, a well-known semiconductor used in high power, high frequency applications, is emerging as one of the earth-abundant two-dimensional materials, employed widely for electronic and optoelectronic purposes.¹ Monolayer SiP is thought to be a promising substance for future nano-electronic and nano-optoelectronic devices.² Silicon phosphide materials have attracted interest as well in the field of energy storage, being employed as anodes for lithium ion batteries.³ Furthermore, the Si:P system is a natural two qubit quantum computer. 4-6 The phosphorus dopant has one electron spin (S = 1/2) and one nuclear spin (I = 1/2), which produces four possible eigenstates. The quantum behavior can be varied as well with phosphorus concentration and temperature.7

SiP could also have important implications for astrochemistry. Several molecular species containing phosphorus, such as CCP, CP, PN, and PH₃, have been identified in carbon-rich circumstellar envelopes, including the famous object IRC+10216.8,9 Siliconbearing species are even more common in such envelopes, such as SiC, SiCN, SiS, and SiC2.10 The envelopes of oxygen-rich stars also contain compounds of these types, including PO and SiO.11 It is, therefore, likely that molecules with an Si-P bond would be present in sources like IRC+10216; however, to date, none have been detected. As for many possible interstellar molecules, this phenomenon is in part due to the lack of experimental spectra crucial for astronomical identification.

The molecule with the simplest silicon-phosphorus system, SiP, has been the subject of many theoretical investigations since the early 1980s. 12-16 Using a multitude of methods, including multireference configuration interaction (MRD-CI), singles and

^{a)}Author to whom correspondence should be addressed: markburton@arizona.edu

doubles configuration interaction including Davidson's correction [CISD(Q)], complete active space self-consistent field (CASSCF), and multireference singles and doubles configuration interaction including Davidson's correction [MRCISD(Q)], these studies primarily examined the low-energy $^2\Pi/^2\Sigma$ electronic state system. Among the quantities computed were potential energy curves, vibrational frequencies, spectroscopic constants, dipole moment functions, oscillator strengths, and Franck–Condon factors. The general agreement has been that the $^2\Pi_{\rm i}$ term is the ground electronic state, with the nearby $A^2\Sigma^+$ state lying ~470 cm $^{-1}$ higher in energy. 16

Despite the many computational studies, it was not until 2002 that an experimental investigation of the SiP molecule was successfully conducted. Using Laser Induced Fluorescence (LIF) spectroscopy, Jakubek et al. were the first to observe this radical in the gas-phase.¹⁷ They created the molecule in a supersonic expansion by laser ablation of a silicon rod in the presence of PH₃, seeded in helium. These authors confirmed the $X^2\Pi_i$ ground state and observed both the $A^2\Sigma$ - $X^2\Pi$ and $B^2\Sigma$ - $X^2\Pi$ transitions at high resolution. They determined rotational, fine structure, and vibrational constants, along with excited state energies and Frank-Condon factors. Jakubek et al.17 found that the A excited state lies 427.4(5) cm⁻¹ above the ground state, close to the value predicted by theory. They also found the $\Omega = 1/2$ ladder in the v = 0 level of the ground state to be perturbed. They suggested that the close-lying A state is perturbing the ground state through ${}^2\Pi/{}^2\Sigma$ spin–orbit interactions.¹⁸ The authors conducted a deperturbation analysis of all observed vibrational levels of the A and X states, establishing unperturbed values for the spin-orbit constant A, the off-diagonal term AAX, and vibrational parameters. No further experimental studies followed this important work.

Here, we present the first pure rotational study of the SiP radical ($X^2\Pi_i$). Using millimeter-wave direct absorption methods, over twelve rotational transitions were recorded arising from each of the $\Omega=3/2$ and 1/2 spin–orbit components. In contrast to the LIF work, the molecule was created in a bulb-type synthesis by the reaction of phosphorus vapor and SiH4. Rotational, spin–orbit, lambda-doubling, and phosphorus hyperfine constants were determined for SiP in the $X^2\Pi$ state from these data. Perturbations were observed in the $\Omega=1/2$ ladder, which, along with the data of Jakubek et al., 17 allowed for a deperturbation analysis of the ground state. A discussion of the astronomical implications of the laboratory work on SiP is given elsewhere. 19 In this paper, we present our spectra, analyses of the data, including the rotational perturbations, interpretation of the hyperfine constants, and a discussion of the bonding in this interesting radical.

II. EXPERIMENTAL

Pure rotational spectra of the SiP radical $(X^2\Pi_i)$ were recorded using one of the millimeter-wave direct absorption spectrometers of the Ziurys group. Briefly, radiation in the range of 65–140 GHz, produced by one of several WR-12, WR-10, and WR-8 Gunn oscillators, is coupled to a Schottky diode varactor multiplier (doubler, triplers, quadruplers) to generate higher frequencies (~130–850 GHz). The radiation is passed quasioptically using a feedhorn and several lenses through a 1 m long, glass reaction cell and into a helium-cooled InSb hot electron bolometer detector. Attached

to one end of the cell is a removable glass hemisphere, enclosed in a heating mantle, for phosphorus vapor production. Within the cell, two cylindrical electrodes are attached to support a longitudinal AC discharge. Frequency modulation of the Gunn oscillator at a rate of 25 kHz is employed for phase-sensitive detection; signals are processed at 2f using a lock-in amplifier. More details can be found in Savage and Ziurys. 20

The SiP radical was synthesized by the reaction of gas-phase phosphorus, produced by heating the solid, red form of this element, and SiH₄/Ar in an AC discharge. Optimized signals were produced when the phosphorus was heated to 480 $^{\circ}$ C and 30 mTorr of \sim 0.8% SiH₄ in argon was used. The AC discharge power was 250 W with an impedance of 600 Ω . Addition of more SiH₄ helped in improving the molecular signals but resulted in an unstable discharge. This successful synthesis method also produced a white phosphorous residue, which is highly flammable. Therefore, extreme caution was taken when venting and cleaning the reaction cell.

Molecular transition frequencies were measured using scans 5 MHz wide in frequency, centered at a given line. Because of the closely blended features, an average of four scans (two in ascending and two in descending frequency) were typically needed to achieve a reasonable signal to noise level. Features below 300 GHz needed more averages as the sensitivity of the detector is lower. The estimated experimental accuracy is $\pm 50~\mathrm{kHz}.$

III. RESULTS

The LIF work of Jakubek et al. 17 enabled the rotational transitions of the $X^2\Pi_i$ state to be predicted. Based on these values, ~20 GHz was continuously scanned (~2.5 B) several times near 350 GHz, with new synthesis conditions each iteration. A closely spaced doublet was subsequently found near 342 GHz, which appeared to be slightly further split into a "doublet of doublets" (see Fig. 1, lower panel); these features were ~3 GHz higher in frequency than predicted. The main doublet separation was a few MHz, and thus, it was assumed it arose from lambda-doubling in the Ω = 3/2 ladder, with the additional splitting due to phosphorus hyperfine interactions $[I(^{31}P) = 1/2]$. A set of doublets with a much larger separation of ~450 MHz was then found to be ~900 MHz higher in frequency and was assigned to the $\Omega = 1/2$ component. Evidence of hyperfine also was present in these features, as shown in Fig. 2, although more prominent in one lambda doublet, f, as illustrated in the inset. All observed lines required the presence of both SiH₄ and phosphorous vapor. Transitions higher in *J* were then predicted and found, following a similar doublet spectral pattern for the Ω = 3/2 and 1/2 components, with a rotational constant that matched that of SiP from the LIF study within the uncertainties. The lambda-doubling for the Ω = 3/2 state steadily increased from ~0.2 MHz at $J = 9.5 \leftarrow 8.5$ to ~6 MHz at $J = 33.5 \leftarrow 32.5$, as expected for a ${}^{2}\Pi$ state. It also became clear that the $\Omega = 1/2$ ladder was perturbed, as found by Jakubek et al. 17 The f lambda doublet appeared to shift to higher frequencies than harmonically-predicted with consecutive J. These data were sufficient evidence for the presence

Figure 1 shows the evolution of the lambda-doubling and hyperfine splitting at higher J (>340 GHz), and Fig. 3 to lower J, both in the Ω = 3/2 ladder, measured in this work. In Fig. 1, the J = 23.5 \leftarrow 22.5 (top), J = 22.5 \leftarrow 21.5 (middle), and J = 21.5 \leftarrow 20.5 (lower)

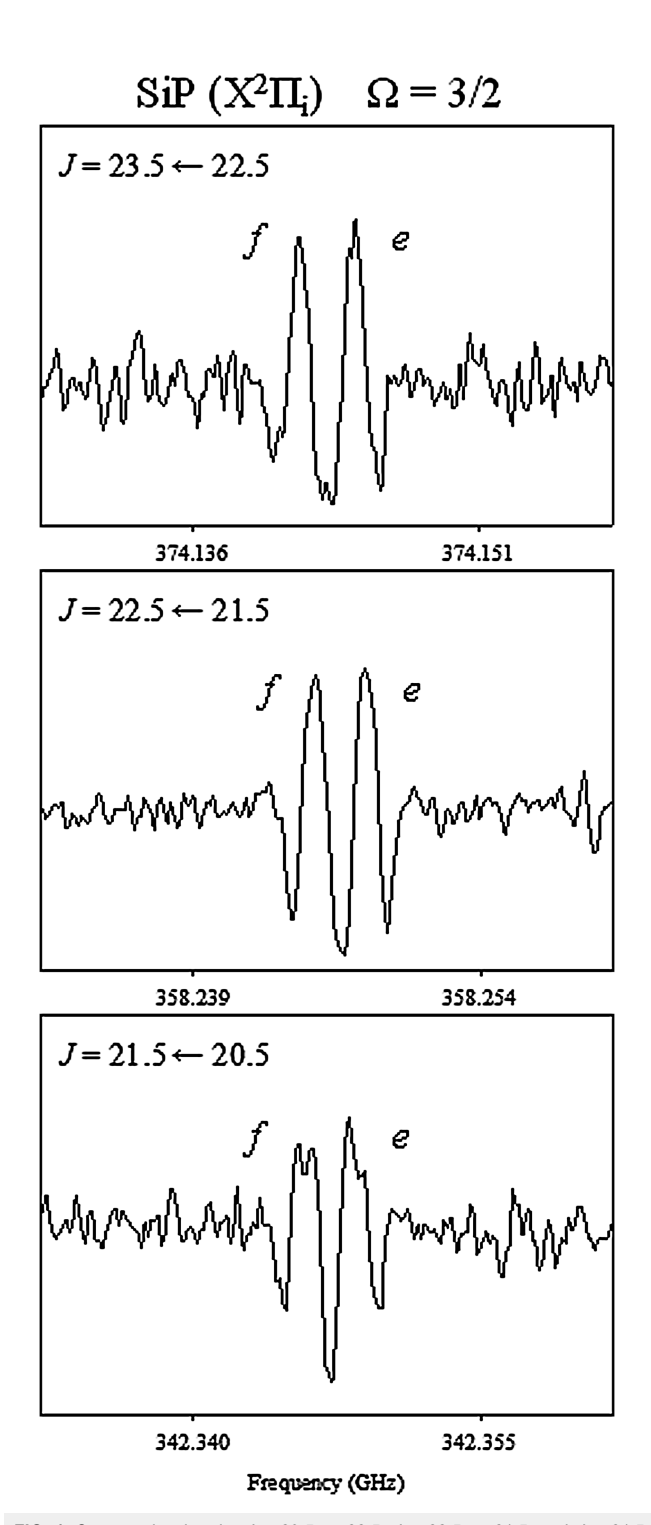


FIG. 1. Spectra showing the $J=23.5\leftarrow22.5$, $J=22.5\leftarrow21.5$, and $J=21.5\leftarrow20.5$ rotational transitions of SiP (X $^2\Pi_i$) in the $\Omega=3/2$ ladder near 374, 358, and 342 GHz, respectively. The lambda-doublets are visible in the data, separated by \sim 3 MHz, labeled by e and f. The hyperfine interactions, arising from the nuclear spin of phosphorous (I=1/2), are slightly resolved in the $J=21.5\leftarrow20.5$ transition (lower panel). Each spectrum was collected in one \sim 70 s scan and truncated to 30 MHz.

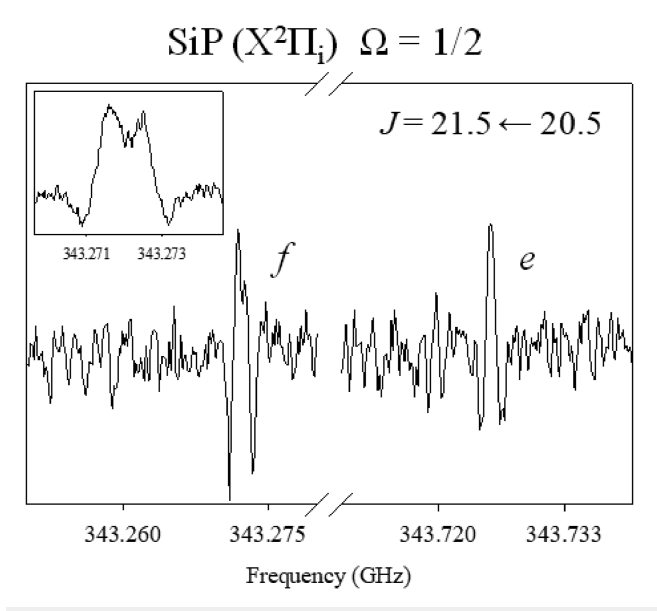


FIG. 2. Spectrum of the $J=21.5\leftarrow20.5$ rotational transition of SiP $(X^2\Pi_i)$ in the $\Omega=1/2$ ladder near 343 GHz. There is a frequency break in the data in order to show the lambda-doublets, which are separated by ~650 MHz and labeled by e and f. Each spectrum was truncated from a 110 MHz scan recorded in 70 s. The f component appears to be slightly split into hyperfine doublets, due to the phosphorus spin. This splitting is more evident in a higher-resolution scan, as shown in the inset, recorded over a 5 MHz range with higher sampling. In general, the phosphorous hyperfine splitting is more readily observed in the f component in the $\Omega=1/2$ ladder.

rotational transitions near 374, 358, and 342 GHz, respectively, are displayed on the same frequency scale. The lambda-doublets, separated by \sim 3 MHz, are labeled by e and f. The figure shows that, as J increases, the small phosphorus hyperfine splitting, seen in the $J=21.5 \leftarrow 20.5$ transition, collapses, while the lambda-doubling slightly increases.

The e/f labeling was done on the basis that for a net $^2\Sigma^+$ perturber, the + parity state should lie lower in energy than the – state. For half-integer J, the e and f designations are $(-1)^{J-1/2}$ and $(-1)^{J+1/2}$, respectively. The f level is, therefore, lower in energy than the e level, as also found by Jakubek et al. This assignment places the f component lower in frequency.

Figure 3 displays the $J=16.5\leftarrow15.5$ (upper), $J=15.5\leftarrow14.5$ (middle), and $J=14.5\leftarrow13.5$ (lower) rotational transitions of SiP near 263, 247, and 231 GHz, respectively, in the $\Omega=3/2$ ladder, measured in this work. The e/f assignment of the lambda-doublets is given by the dashed/bold lines underneath the spectra; hyperfine components are labeled by quantum number F, where F=J+I, and I=1/2. At the lower frequencies shown here, the hyperfine interactions have increased, first creating a sharp triplet (upper panel), then a triplet with a broader central feature (middle panel), and then a distinct quartet (lower panel). In the lower spectrum, the magnitude of the hyperfine and lambda-doubling interactions is almost identical, interspersing the hyperfine components of opposite lambda-doublets.

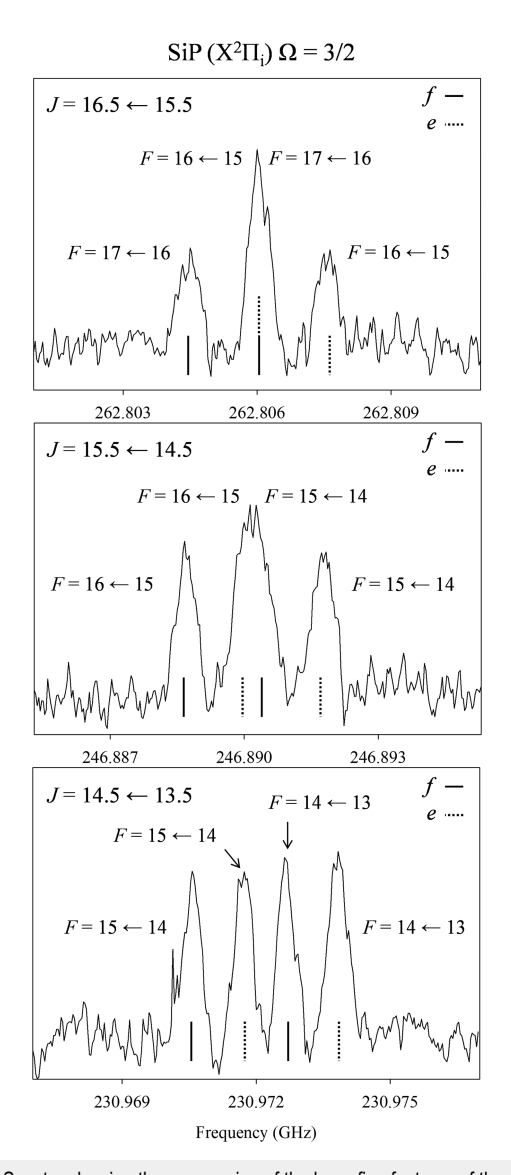


FIG. 3. Spectra showing the progression of the hyperfine features of the J=16.5 ← 15.5, J=15.5 ← 14.5, and J=14.5 ← 13.5 rotational transitions of SiP ($X^2\Pi_i$) in the $\Omega=3/2$ ladder near 262, 247, and 231 GHz, respectively. The hyperfine transitions are labeled by quantum number F, and the lambda-doublets by solid (f) and dashed (e) lines underneath the spectra. In the higher frequency transition (J=16.5 ← 15.5, upper panel), the combination of hyperfine and lambda-doublets produces a "triplet," with the center feature being a blend of the F=16 ← 15 f and F=17 ← 16 e components. As the frequency decreases, these blended lines start to separate (J=15.5 ← 14.5, middle panel). At lower frequencies (J=14.5 ← 13.5, lower panel), the blended feature disappears as F=14 ← 13 f and F=15 ← 14 e components cross each other, creating a "doublet of doublets." Each spectrum is an average of 6 scans, 70 s in duration and 10 MHz wide, half ascending in frequency and half descending in frequency.

In total, frequencies in 15 rotational transitions, $J+1 \leftarrow J$, were measured in the $\Omega=3/2$ ladder, and twelve for the $\Omega=1/2$ component. The measured transition frequencies are listed in Table I. As shown in the table, each rotational transition is split

into lambda-doublets, indicated by e and f; furthermore, most were additionally split into hyperfine components, indicated by F. In some cases, the hyperfine structure was blended into a single, broad feature (e.g., Fig. 3), and the frequencies were determined by Gaussian fits to the line profiles. Over 70 individual lines were measured.

IV. ANALYSIS

The data were fit with a Hund's case (a_{β}) effective Hamiltonian using $Hund\ A$, a program originally developed by Brown and collaborators, and further modified in the Ziurys group. Basic matrix elements are given in Ref. 21. Because of obvious perturbations, only some of the $\Omega=1/2$ measurements (J<27.5; see Table I) were included in the analysis. The Hamiltonian consisted of rotational, spin–orbit, lambda-doubling, and magnetic hyperfine terms,

$$\mathbf{H}_{\text{eff}} = \mathbf{H}_{\text{rot}} + \mathbf{H}_{\text{SO}} + \mathbf{H}_{\text{LD}} + \mathbf{H}_{\text{mhf}}. \tag{1}$$

In the fit, the spin-orbit constant, A, was held fixed to that determined in the previous optical work, 17 but the centrifugal distortion corrections were varied. Both A_H and A_D were found to be necessary for a good fit. In addition to p and q (or p + 2q and q), the lambda-doubling required higher order centrifugal distortion parameters $(p + 2q)_D$ and $(p + 2q)_H$, which were both well-determined. For the hyperfine analysis, all four Frosch and Foley²² parameters (a, b, c, and d) were initially fit; however, d could not be determined beyond a 2σ uncertainty and was, therefore, fixed to that initial value (-760 MHz) in the final analysis. Higher order centrifugal distortion corrections to the hyperfine interactions were additionally employed, but did not improve the fit, and were, therefore, not included. The need for higher-order distortion constants $[A_H]$ $(p + 2q)_H$ most likely is a result of the perturbation at higher I. The resulting spectroscopic constants are given in Table II. The rms of the fit is 62 kHz, within the estimated experimental uncertainty. Using these values, transitions down to $J = 3.5 \leftarrow 2.5$ (~55 GHz) were predicted and given for reference as Table SI in the supplementary material.

Also shown in Table II are the constants for SiP for the ground $^2\Pi$ state from the LIF¹⁷ measurements. These values are in reasonable agreement with the millimeter-wave data; however, the lambda-doubling parameter q is about an order of magnitude larger in the LIF fit and has a positive sign. According to pure precession, the sign of q should be negative for a positive p. 23 We attribute these differences to experimental resolution and the difficulties in analyzing perturbed spectra.

A $^2\Pi/^2\Sigma$ deperturbation analysis was also performed for SiP for the rotational levels of the ground electronic state, v=0 level. An energy level diagram illustrating the A–X interaction is shown in Fig. 4. The $^2\Pi/^2\Sigma$ interaction is thoroughly discussed by Lefebvre-Brion and Field¹⁸ and has been applied for other molecules, such as CN and CS⁺. 24,25 The energy expressions used in the analysis for the $X^2\Pi/A^2\Sigma^+$ interaction are given in Table III. Note that the $^2\Sigma$ matrix element contains only B₀ and γ , because centrifugal distortion terms were not experimentally measured¹⁷ for SiP for this state. The two deperturbation parameters $a_+/2$ and B_vb , following the selection rule $\Delta\Omega=0$, arise from

TABLE I. Observed transitions for SiP ($X^2\Pi_i$).^a

					$\Omega = 3/2$		$\Omega = 1/2$	
J'	F'	J"	F"	Parity	$\mathbf{v}_{\mathrm{obs}}$	obs – calc	$\mathbf{v}_{\mathrm{obs}}$	obs – calc
9.5	10	8.5	9	f	151 351.095	0.066		
	10		9	e	151 351.538	0.009		
	9		8	f	151 356.500	0.037		
	9		8	e	151 356.912	-0.081		
14.5	15	13.5	14	f	230 970.567	-0.034	231 515.275	-0.067
	15		14	e	230 971.745	-0.021		
	14		13	f	230 972.709	0.095	231 516.554	0.036
	14		13	e	230 973.790	-0.036		
15.5	16	14.5	15	f	246 888.654	-0.051	247 488.202	-0.045
	16		15	e	246 890.020	-0.015		
	15		14	f	246 890.498	0.099	247 489.439	0.100
	15		14	e	246 891.731	-0.047		
16.5	17	15.5	16	f	262 804.558	-0.008	263 458.787	-0.056
	17		16	e	262 806.060	-0.010		
	16		15	f	262 806.060	0.063	263 459.895	0.028
	16		15	e	262 807.548	-0.006		
20.5	21	19.5	20	f	326 442.748	-0.061	327 314.899	-0.027
	20		19	f	326 443.630	0.086	327 315.792	0.018
	21		20	e	326 445.034	-0.074	327 772.694	0.090
	20		19	e	326 445.945	0.037	327 773.221	-0.123
21.5	22	20.5	21	f	342 345.318	-0.051	343 271.590	0.021
	21		20	f	342 346.111	0.123	343 272.401	0.013
	22		21	e	342 347.855	-0.034	343 724.952	0.134
	21		20	e	342 348.622	0.046	343 725.462	-0.071
22.5	23	21.5	22	f	358 244.755	-0.091	359 224.965	0.027
	22		21	f	358 245.380	0.017	359 225.684	-0.048
	23		22	e	358 247.593	-0.004	359 673.718	0.084
	22		21	e	358 248.101	-0.085	359 674.212	-0.113
23.5	24	22.5	23	f	374 141.078	-0.020		
	23		22	f	374 141.578	0.051		
	24		23	e	374 144.123	0.033		
	23		22	e	374 144.632	0.039		
27.5	28	26.5	27	f	437 691.076	0.053		
	27		26	f	437 691.106	-0.081		
	28		27	e	437 695.146	0.091		
	27		26	e	437 695.176	-0.130		
28.5	29	27.5	28	f	453 569.080	0.060	454 869.155	b
	28		27	f	С	-0.055	С	b
	29		28	e	453 573.437	0.104	455 287.045	b
	28		27	e	С	-0.100	С	b
29.5	30	28.5	29	f	469 442.977	0.038	470 795.543	b
	29		28	f	С	-0.032	С	b
	30		29	e	469 447.603	0.064	471 207.939	b
					405 447.003 c	-0.099	4/1 20/.939 c	ь
20.5	29	20.5	28	e	405 212 620		406 717 400	b
30.5	31	29.5	30	f	485 312.639	0.003	486 717.492	b
	30		29	f		-0.027		b
	31		30	e	485 317.622	0.090	487 124.223	b
	30		29	e		-0.035		
31.5	32	30.5	31	f	501 177.950	-0.020	502 634.802	b
	31		30	f	С	-0.013	С	b
	32		31	e	501 183.202	0.035	503 035.767	b
	31		30	e	С	-0.057	c	b

TABLE I. (Continued.)

					$\Omega =$	$\Omega = 3/2$		$\Omega = 1/2$	
J'	F'	J‴	F"	Parity	$\mathbf{v}_{\mathrm{obs}}$	obs – calc	$\mathbf{v}_{\mathrm{obs}}$	obs – calc	
32.5	33	31.5	32	f	517 038.771	-0.025	518 547.325	b	
	32		31	f	С	0.015	С	b	
	33		32	e	517 044.343	0.040	518 942.475	b	
	32		31	e	С	-0.021	С	b	
33.5	34	32.5	33	f	532 894.938	-0.034	534 454.922	b	
	33		32	f	С	0.037	С	b	
	34		33	e	532 900.838	0.041	534 844.161	b	
	33		32	e	c	0.009	c	b	

^a All values in MHz.

spin-orbit and spin-electronic interactions, respectively. They are defined as

$$\frac{a+}{2} = \langle ^2 \Sigma | A \mathbf{L}_- |^2 \Pi \rangle, \tag{2}$$

$$B_{\nu}b = \langle^{2}\Sigma|B(R)\mathbf{L}_{-}|^{2}\Pi\rangle. \tag{3}$$

There are also *L*-uncoupling terms contributing to $B_{\nu}b$, as will be discussed. Here, it is assumed that the $^2\Pi$ and $^2\Sigma$ states have the same potential curves, which is a reasonable approximation (see Jakubek *et al.*¹⁷), and that $\langle v_{\sigma}|v_{\pi}\rangle=1.^{18}$ The two states must also arise from π^1 (in this case π^3) and σ^1 electron configurations and differ by one spin-orbital—another criteria for the $^2\Pi/^2\Sigma$ interaction. Note

TABLE II. Spectroscopic constants for SiP $(X^2\Pi_i)$.

Parameter	mm-wave	$\mathrm{LIF}^{\mathrm{b}}$	
В	7980.696 2(81)	7928(28)	
D	0.006 207 5(86)	0.038(30)	
A	-5599344°	-5 599 344(990)	
A_D	-4.598(16)	2.5(1.6)	
A_{H}	0.000 381(17)	• • •	
p+2q	507.5(2.3)	• • •	
$(p+2q)_D$	-0.0407(39)	• • •	
$(p+2q)_H$	0.000 004 8(30)	• • •	
p	508.1(2.3)	554(171)	
q	-0.2960(88)	68(42)	
a	309(38)		
b	354(51)		
b+c	96(86)		
c	-258(85)		
d	-760^{d}	•••	
rms	0.062		

^a All values in MHz; errors are 3σ.

that in the case of SiP, the Π state lies lower in energy whereas most treatments have the Σ state being lower (e.g., for CN and CS⁺). ^{24,25} In this analysis, the hyperfine structure of SiP was not considered, and the frequencies of the phosphorus doublets were simply averaged. The hyperfine-free frequencies are listed in Table IV, including the residuals from the fit, which include the perturbed higher I transitions of the Ω = 1/2 component that were excluded from the previous case (a_{β}) analysis. The rotational, centrifugal distortion, spin–orbit A_D , and lambda doubling terms $(p, p_D, \text{and } q)$ were allowed to float for the $\mathbf{X}^2\Pi$ state while A, $\Delta E_{\Pi/\Sigma}$ ($T_0^{-\Pi} - T_0^{-\Sigma}$), and the rotational and spin-rotation constants (B^{Σ} and y^{Σ}), were held fixed to the values determined by Jakubek *et al.*¹⁷ The measured transitions were not given by Jakubek *et al.*¹⁷ for the A state and, as such, could not be incorporated into this analysis. Therefore, as mentioned, the rotational and spin-rotation terms were fixed. Higher order centrifugal distortion terms were not necessary (e.g., A_H , p_H , and q_D), as they likely compensate for the perturbation.

The resulting deperturbed spectroscopic constants are given in Table V. The rms of the fit is 46 kHz, excluding the $J=9.5 \leftarrow 8.5$

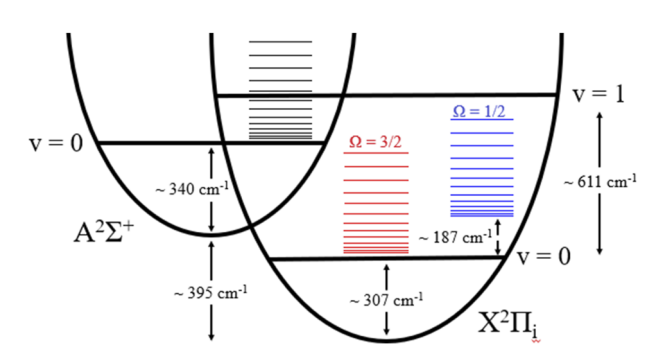


FIG. 4. Qualitative energy level diagram of SiP, showing the v = 0 levels of the $X^2\Pi_1$ and $A^2\Sigma^+$ states, based on vibrational constants given in Jakubek *et al.* The rotational level manifolds are displayed for the A state (in black) as well as the $\Omega=3/2$ and 1/2 ladders in the ground state (in red and blue, respectively). The rotational levels of the A state and those observed in the $X^2\Pi_{1/2}$ sub-state are close in energy and interact.

^bValues not included in fit.

 $^{^{\}rm c}$ Hyperfine unresolved.

^bFrom Jakubek *et al*.¹¹

cHeld fixed to Jakubek et al.;17 see the text.

^dHeld fixed; see the text.

TABLE III. Rotational energy matrix for the $A^2\Sigma^+/X^2\Pi_i$ interaction.^a

	$^2\Pi_{1/2}$	$^2\Pi_{3/2}$	$^2\Sigma^+$
$^2\Pi_{1/2}$	$\begin{split} T_0 - {}^1\!/2A + (B - A_D)(J + {}^1\!/2)^2 \\ - D \left[(J + {}^1\!/2)^4 + (J + {}^1\!/2)^2 - 1) \right] \mp {}^1\!/2[p \\ + p_D J(J + 1)](J + {}^1\!/2 \mp 1) + {}^1\!/2q(J + {}^1\!/2 \mp 1)^2 \end{split}$	$-[B-2D((J+1/2)^2-1)+\\1/4[p+p_DJ(J+1)]\mp1/2q(J+1/2\mp1)][(J+1/2)^2-1]^{1/2}$	$a_{+}/2 \mp B_{v}b(J + 1/2 \mp 1)$
$^{2}\Pi_{3/2}$	Symmetric	$\begin{split} &T_0 + {}^1\!/2A + (B + A_D)[(J + {}^1\!/2)^2 - 2] - D \\ &[(J + {}^1\!/2)^4 - 3(J + {}^1\!/2)^2 + 3] + {}^1\!/2q[(J + {}^1\!/2)^2 - 1] \end{split}$	$-B_{v}b[(J+1/2)^{2}-1]^{1/2}$
$^2\Sigma^+$	Symmetric	Symmetric	$T_0^{\Sigma} + B^{\Sigma}(J + 1/2)(J + 1/2 \mp 1)$ $\pm 1/2\gamma(J + 1/2 \mp 1)$

^aHyperfine not included; from Lefebvre-Brion and Field. ¹⁸

transition only. As the table shows, B changes by <1 MHz, while A_D becomes positive and decreases by a factor of ~10, perhaps expected as the perturbation is considered. The lambda-doubling constant p shows the largest difference, which decreases from 507 to 178 MHz; q is reduced by a factor of ~2. Such decreases are consistent with the

TABLE IV. Frequencies for deperturbation analysis of SiP $(X^2\Pi_i)$.^a

			$\Omega = 3/2$		$\Omega =$	1/2
J′	J′′	Parity	$\mathbf{v}_{\mathrm{obs}}$	obs – calc	$\mathbf{v}_{\mathrm{obs}}$	obs – calc
14.5	13.5	f	230 971.638	0.087	231 515.915	-0.067
		e	230 972.768	0.068		
15.5	14.5	f	246 889.576	0.058	247 488.821	-0.001
		e	246 890.876	0.046		
16.5	15.5	f	262 805.309	0.042	263 459.341	-0.013
		e	262 806.804	0.052		
20.5	19.5	f	326 443.189	-0.026	327 315.346	0.058
		e	326 445.490	-0.006	327 772.958	-0.064
21.5	20.5	f	342 345.715	-0.010	343 271.996	0.051
		e	342 348.239	0.009	343 725.207	0.007
22.5	21.5	f	358 245.068	-0.090	359 225.325	-0.036
		e	358 247.847	-0.051	359 673.965	-0.014
23.5	22.5	f	374 141.328	-0.043		
		e	374 144.378	0.023		
27.5	26.5	f	437 691.091	-0.064		
		e	437 695.161	-0.050		
28.5	27.5	f	453 569.080	-0.037	454 869.155	0.014
		e	453 573.437	-0.027	455 287.045	0.035
29.5	28.5	f	469 442.977	-0.022	470 795.547	-0.002
		e	469 447.603	-0.043	471 207.939	0.060
30.5	29.5	f	485 312.639	-0.018	486 717.492	0.006
		e	485 317.622	0.008	487 124.223	0.044
31.5	30.5	f	501 177.950	0.003	502 634.802	0.004
		e	501 183.202	-0.020	503 035.767	0.002
32.5	31.5	f	517 038.771	0.045	518 547.325	-0.008
		e	517 044.343	0.016	518 942.475	-0.020
33.5	32.5	f	532 894.938	0.087	534 454.922	-0.018
		e	532 900.838	0.051	534 844.161	-0.063

 $^{^{\}mathrm{a}}$ All values in MHz; hyperfine splittings collapsed.

deperturbation. The values for the deperturbation parameters are $a_+/2 = 22.66(10) \text{ cm}^{-1}$ and $B_\nu b = -0.1011(37) \text{ cm}^{-1}$. These values are comparable to what has been found for CS⁺, for example. Anote that Jakubek *et al.* Found that the off-diagonal spin-orbit term $A_{AX} = a_+ = 45(5)$ or 51(8) cm⁻¹, depending on the method, in excellent agreement with our value $a_+ = 45.32(20) \text{ cm}^{-1}$, where $a_+ = \langle \sigma | al_- | \pi \rangle$.

V. DISCUSSION

A. Confirmation of the $^2\Pi_i$ ground state and bonding perspective

This work clearly supports the results of Jakubek *et al.*,¹⁷ and confirms the $^2\Pi_i$ ground electronic state for SiP. The inverted designation is evident in the observed lambda-doubling, with the larger splitting in the less intense harmonic pattern, consistent with the $\Omega=1/2$ ladder lying higher in energy. As found by Jakubek *et al.*, the $\Omega=1/2$ manifold is clearly perturbed, noticeable around $J\sim22.5$ in our spectra, or at an energy of $BJ(J+1)+A\sim330~{\rm cm}^{-1}$ — consistent with the A–X energy separation of $\sim427~{\rm cm}^{-1}$. Furthermore,

TABLE V. Deperturbed spectroscopic constants for SiP $(X^2\Pi_i)$.^a

Parameter	Value		
$T_0^{\Pi} (cm^{-1})$	0_{p}		
$A (cm^{-1})$	$-186.774^{\rm b}$		
A_{D}	0.626(21)		
В	7 979.104(58)		
D	0.006 065 2(31)		
p	178(27)		
p_{D}	-0.0133(23)		
q	-0.137(43)		
$a_{+}/2 \text{ (cm}^{-1})$	22.66 (10)		
$b_v B (cm^{-1})$	-0.1011(37)		
T_0^{Σ} (cm ⁻¹)	427.4 ^b		
B^{Σ}	8 869.6 ^b		
γ^{Σ}	$-10972.4^{\rm b}$		
rms	0.046		

 $^{^{\}text{a}}\text{In MHz}$ unless stated otherwise; uncertainties are 3σ , hyperfine not included.

^bHeld fixed from Jakubek *et al.*¹³

the off-diagonal spin orbit correction is comparable, as mentioned (\sim 45 cm $^{-1}$).

The electron configuration that gives rise to this $X^2\Pi_i$ state is $\sigma^2\pi^3$. $A^2\Sigma^+$ is created from promoting a σ electron into the π orbital, $\sigma^1\pi^4$. As discussed by Ornellas *et al.*, ¹⁶ these two states share the same dissociation limit, with the atoms in $Si(^3P)$ and $P(^4S)$ states. The silicon 3P term must arise from a p^2 configuration, while for phosphorus, p^3 . These p orbitals form the valence σ and π orbitals, and, therefore, the $X^2\Pi_i$ and $A^2\Sigma^+$ states differ by one spin-orbital. For SiP, as well as the P_2^+ ion, ¹³ the π orbital is higher in energy than the σ and, therefore, contains the unpaired electron. It is the opposite for the lighter isovalent molecules, SiN, CP, and CN, which have the unpaired electron in the higher energy σ orbital and a $X^2\Sigma^+$ ground state. ¹⁶ The change in energy ordering is attributed to orbital stability as the periodic table is descended. ¹³

The bond length of SiP using the deperturbed rotational constant is $r_0 = 2.076$ Å. Although not corrected for zero-point vibrations, this value is typical for Si=P double bonds, which is 2.07 Å. ²⁶ It is also consistent with other molecules with this double bond, such as HPSi $(2.045 \text{ Å})^{27}$ and SiPH₃ (2.075 Å). ²⁶ As discussed by Baboul *et al.*, ²⁶ the typical single Si–P bond length is significantly longer (2.25 Å), and the estimated triple SiP bond is \leq 1.933 Å. ²⁸ The SiP bond length determined here also compares reasonably well with the equilibrium bond length of $r_e = 2.089 \text{ Å}$ from theoretical calculations. ¹⁶

B. Interpretation of the deperturbation analysis and implications for pure precession

As discussed previously, the constant that varies the most from the perturbed to deperturbed fit is p, which decreases in value from 508.1(2.3) to 178(27) MHz, respectively. It is clear that the large value of this parameter, as well as the need for higher centrifugal distortion constants, was a compensation for the perturbation. A_D also changes noticeably, from -4.598(16) to 0.626(21) MHz. Again, the decrease in value, and even the sign change, suggests that A_D was also accounting for the perturbation.

The ${}^2\Pi/{}^2\Sigma$ interaction arises from spin-orbit and spin-electronic coupling between the two states, which both follow the $\Delta\Omega=0$ selection rule and are manifested in constants a_+ and b. The $\Omega=3/2$ levels are thus unaffected by this coupling. There is also a contribution from the L-uncoupling operator BJ_+L_- , which connects the ${}^2\Pi_{1/2}$ and ${}^2\Pi_{3/2}$ sub-states with the $\Omega=-1/2$ and +1/2 components, respectively, of the ${}^2\Sigma$ state. In this case, $\Delta\Omega=\pm 1$, adding additional terms related to b to the interaction.

The pure precession approximation really applies only to diatomic hydrides, where the outer electrons act as if they were in an atom formed by the two nuclei. In that case, the atomic angular momentum l is well-defined. However, some insight from pure precession can be gained for molecules other than hydrides; for example, signs of the lambda-doubling constants, as discussed by Mulliken and Christy. In the pure precession approximation, the deperturbation constants take on special meaning, 18,23

$$a+=[l(l+1)]^{1/2}A,$$
 (4)

$$b = [l(l+1)]^{1/2}. (5)$$

Here, A is the spin–orbit constant of the ${}^2\Pi/{}^2\Sigma$ pair and l is the atomic angular momentum of the valence σ and π electrons (l=1 for SiP). These expressions lead to the well-known equations for the lambda-doubling terms p and q_2^{23}

$$p = 2AB[l(l+1)]^{1/2}/(E_{\Pi} - E_{\Sigma}),$$
 (6)

$$q = 2B^{2}[l(l+1)]^{1/2}/(E_{\Pi} - E_{\Sigma}).$$
 (7)

In the case of SiP, B is the rotational constant for the ground state and $E_{\Pi} - E_{\Sigma}$ is the energy difference in the ${}^2\Pi/{}^2\Sigma$ pair, measured to be ${\sim}427~\text{cm}^{-1}.^{17}$ Because SiP has an inverted Π ground state, A < 0 and $E_{\Pi} - E_{\Sigma} < 0$. Therefore, the sign of p should be positive and that of q should be negative, 23 as has been found. Furthermore, the "deperturbed" ratio $p/q \sim 1300$ is within a factor of 2 of $A/B \sim 700$, as opposed to the "perturbed" ratio of $p/q \sim 1700$. In addition, $a_+/b \sim A$ $\sim 45/-0.2 \sim -225$ cm⁻¹, which is not far from the actual spin-orbit constant, $A \sim -187 \text{ cm}^{-1}$. Although these simple relationships do not yield exact values, pure precession is only a rough approximation in the case of SiP, as for NO and BO, as discussed by Mulliken and Christy.²³ Using the values from the deperturbation analysis, it is estimated that the ${}^{2}\Sigma$ state will start to appreciably interact with the ${}^2\Pi_{1/2}$ state near N=6 and J=35.5, while the ${}^2\Sigma-{}^2\Pi_{3/2}$ coupling begins at approximately N = 7 and J = 44.5, as illustrated in Fig. 5.

C. Hyperfine analysis and the Si-P bond

The bond length measured for SiP suggests a double bond between the two atoms. The $^2\Pi$ ground state has a $(core)7\sigma^28\sigma^29\sigma^23\pi^3$ electron configuration, where the valence 9σ and 3π orbitals are created from p atomic orbitals. This bonding scheme is reflected in the hyperfine parameters. The Fermi contact parameter, b_F , is equal to b+c/3=268(63). It is an indicator of the s-character of the orbital containing the unpaired electron, as it is directly proportional to the electron density at the nucleus with the spin. The Fermi contact term for atomic phosphorus is $a_F(P)=13~306~\text{MHz}.^{29}$ The ratio of molecular to atomic Fermi contact values indicates that the unpaired electron resides in an orbital with $\sim 2\%$ atomic s character. This ratio is consistent with the location of the unpaired electron in the π molecular orbital, as calculated by theory. The nonzero percentage of s-character may arise from some mixing with the 8σ orbital, which is 3s in composition.

The hyperfine constant a arises from the nuclear spin-orbit interaction $I \cdot L$ and, therefore, measures the non-sigma orbital character. It provides an estimate of the radial expectation value $\langle 1/r^3 \rangle$,

$$a = g_{\rm g} g_{\rm N} \mu_{\rm R} \mu_{\rm N} \langle 1/r^3 \rangle. \tag{8}$$

Here, g_s is the spin g factor (2.0023), g_N is the nuclear g factor ($g_N = \mu_I \cdot I = 2.632, I = 1/2$), and μ_B and μ_N are the Bohr and nuclear magnetons, respectively. Using Eq. (8), $\langle 1/r^3 \rangle = 1.428$ a.u.⁻³ = 9.63 Å⁻³ for the unpaired electron in SiP. This value indicates that the average distance of this electron from the phosphorus nucleus is ~0.5 Å. Given the bond length of ~2 Å, this result suggests that the unpaired electron is at least partially located on the P nucleus, in a non-sigma (π) orbital.

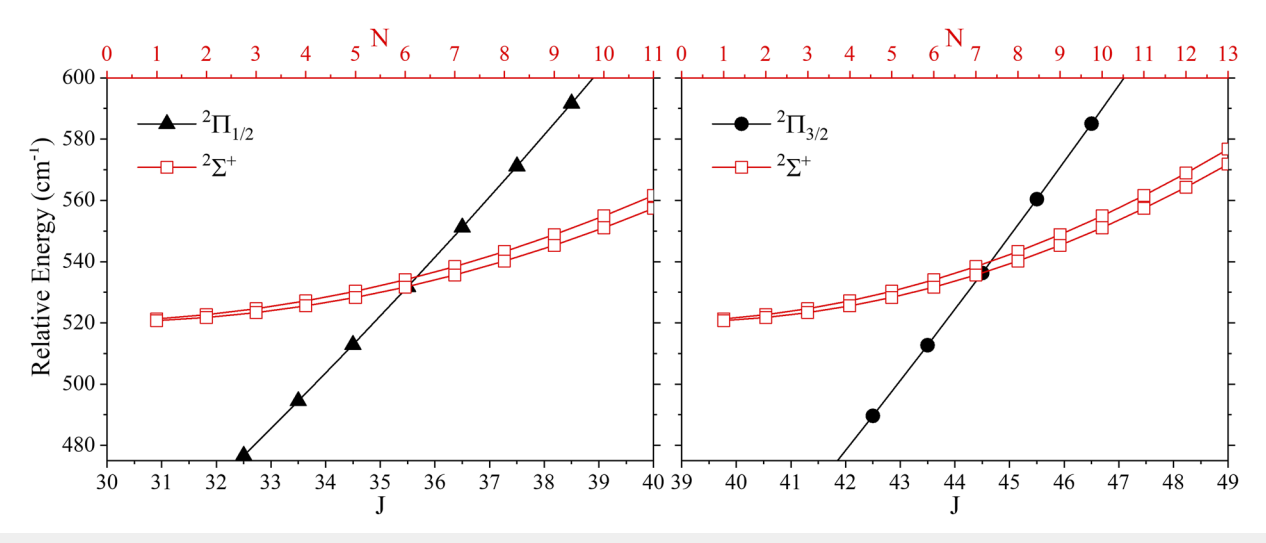


FIG. 5. A diagram showing the rotational energies and the regions of interaction between the $A^2\Sigma^+$ and $X^2\Pi_i$ states as a function of N and J quantum numbers. The ${}^2\Sigma^+/{}^2\Pi_{1/2}$ interaction is shown on the left; the ${}^2\Sigma^+/{}^2\Pi_{3/2}$ interaction is shown on the right. Energies were calculated from the deperturbed rotational parameters for the $X^2\Pi_i$ state (determined here) and the rotational parameters of the $A^2\Sigma^+$ state (from Jakubek *et al.* 17). The ${}^2\Sigma^+$ state crosses the ${}^2\Pi_{1/2}$ substate at approximately J=35.5 (N=6) and the ${}^2\Pi_{3/2}$ substate around J=44.5 (N=7).

The dipolar constant, c, is a measure of non-spherical nature of the orbital of the unpaired electron, 22 and has an associated angular dependence of $((3\cos^2\theta_i-1)/r_i^3)$, namely,

$$c = 3/2g_{s}g_{N}\mu_{R}\mu_{N}\langle(3\cos^{2}\theta_{i}-1)/r^{3}\rangle.$$
 (9)

In the case of SiP, the angular term should arise from the $p\pi$ orbital, which has the value of $\langle (3\cos^2\theta_i-1)\rangle = -2/5$. Using this value for the angular factor and $\langle 1/r^3\rangle = 1.428$ a.u. ³ derived from the *a* hyperfine constant, *c* can be estimated from Eq. (9). From this equation, c=-185 MHz, consistent with the experimentally derived value of c=-258(85) MHz. This agreement supports the proposed electron configuration for the ground state of SiP, $(\cos^2\theta^2 8\sigma^2 9\sigma^2 3\pi^3)$. ¹⁶

VI. CONCLUSIONS

The measurement of the millimeter-wave spectrum of SiP confirms its $X^2\Pi_i$ state and the presence of perturbations of the $\Omega=1/2$ levels, as proposed by previous LIF studies. The deperturbation analysis suggests that the initial, larger value of the lambda-doubling constant p and use of the higher order centrifugal distortion parameters A_H , $(p+2q)_D$, and $(p+2q)_H$ were compensating for such perturbations. The data suggest that the pure precession model can be reasonably applied to SiP, as the electron configurations of the $X^2\Pi$ and $A^2\Sigma$ states differ by one spin-orbital. Analysis of the hyperfine constants, which have been measured for the first time for SiP, is consistent with the location of the unpaired electron in a $p\pi$ orbital, as predicted by the theory. This study served as an excellent benchmark for future computational work of SiP in complex materials.

SUPPLEMENTARY MATERIAL

See the supplementary material for the predicted frequencies of SiP ($X^2\Pi_i$) from 55–532 GHz.

ACKNOWLEDGMENTS

This work was supported by NASA Grant No. 80NSSC18K0584 (Emerging Worlds) and NSF Grant No. AST-1907910.

AUTHOR DECLARATIONS

Conflict of Interest

The authors have no conflicts to disclose.

Author Contributions

All authors contributed equally to this work.

M. A. Burton: Conceptualization (equal); Data curation (equal); Formal analysis (equal); Investigation (equal); Writing – original draft (equal); Writing – review & editing (equal). P. M. Sheridan: Data curation (equal); Formal analysis (equal); Writing – review & editing (equal). L. M. Ziurys: Conceptualization (equal); Formal analysis (equal); Funding acquisition (equal); Supervision (equal); Writing – original draft (equal); Writing – review & editing (equal).

DATA AVAILABILITY

The data that support the findings of this study are available within the article and its supplementary material.

REFERENCES

- ¹ H. Shen, Y. Huang, R. Hao, Y. Chang, Z. Ma, B. Guo, P. Wang, H. Yang, J. Cheng, Q. Li, H. Wang, Z. Liu, and A. Nie, ACS Sustainable Chem. Eng. 8, 17597–17605 (2020).
- ²S. Kansara, P. D. Bhuyan, Y. Sonvane, and S. K. Gupta, J. Mater. Sci. 54, 11878–11888 (2019).
- ³R. Reinhold, U. Stoeck, H.-J. Grafe, D. Mikhailova, T. Jaumann, S. Oswald, S. Kaskel, and L. Giebeler, ACS Appl. Mater. Interfaces 10, 7096–7106 (2018).
- ⁴M. Steger, T. Sekiguchi, A. Yang, K. Saeedi, M. E. Hayden, M. L. W. Thewalt, K. M. Itoh, H. Riemann, N. V. Abrosimov, P. Becker, and H.-J. Pohl, J. Appl. Phys. **109**, 102411 (2011).
- ⁵K. Ambal, P. Rahe, A. Payne, J. Slinkman, C. C. Williams, and C. Boehme, Sci. Rep. **6**, 18531 (2016).
- ⁶L. Zhu, K. J. van Schooten, M. L. Guy, and C. Ramanathan, Phys. Rev. Appl. 7, 064028 (2017).
- ⁷B. E. Kane, Nature **393**, 133–137 (1998).
- ⁸M. Guélin, J. Cernicharo, G. Paubert, and B. E. Turner, Astron. Astrophys. 230, L9–L11 (1990).
- ⁹D. T. Halfen, D. J. Clouthier, and L. M. Ziurys, Astrophys. J. 677, L101–L104 (2008).
- ¹⁰E. D. Tenenbaum, J. L. Dodd, S. N. Milam, N. J. Woolf, and L. M. Ziurys, Astrophys. J. **190**, 348 (2010).
- ¹¹L. M. Ziurys, D. R. Schmidt, and J. J. Bernal, Astrophys. J. **856**, 169 (2018).
- ¹² A. I. Boldyrev, N. Gonzales, and J. Simons, J. Phys. Chem. **98**, 9931–9944 (1994).
- ¹³ P. J. Bruna, H. Dohmann, and S. D. Peyerimhoff, Can. J. Phys. **62**, 1508–1523 (1984).

- ¹⁴R. C. Fortenberry and J. S. Francisco, Astrophys. J. **843**, 124 (2017).
- ¹⁵ A. D. McLean, B. Liu, and G. S. Chandler, J. Chem. Phys. **97**, 8459 (1992).
- ¹⁶F. R. Ornellas, C. M. Andreazza, and A. A. de Almeida, Astrophys. J. **538**, 675 (2000).
- ¹⁷Z. J. Jakubek, S. G. Nakhate, and B. Simard, J. Chem. Phys. 116, 6513 (2002).
- ¹⁸H. Lefebvre-Brion and R. W. Field, Perturbations in the Spectra of Diatomic Molecules (Academic Press, Orlando, 1986).
- 19 L. A. Koelemay, A. P. Singh, M. A. Burton, P. M. Sheridan, J. J. Bernal, and L. M. Ziurys, Laboratory and astronomical detection of the SiP radical (X_2 Πi): More circumstellar phosphorus *Astrophys. J.* (in press).
- ²⁰C. Savage and L. M. Ziurys, Rev. Sci. Instrum. **76**, 043106 (2005).
- ²¹J. Brown and A. Carrington, Rotational Spectroscopy of Diatomic Molecules (Cambridge University Press, 2003).
- ²²R. A. Frosch and H. M. Foley, *Phys. Rev.* **88**, 1337 (1952).
- ²³ R. S. Mulliken and A. Christy, Phys. Rev. **38**, 87 (1931).
- ²⁴D. Gauyacq and M. Horani, Can. J. Phys. **56**, 587 (1978).
- ²⁵ A. J. Kotlar, R. W. Field, J. I. Steinfeld, and J. A. Coxon, J. Mol. Spectrosc. 80, 86–108 (1980).
- ²⁶ A. G. Baboul and H. B. Schlegel, J. Am. Chem. Soc. **118**, 8444–8451 (1996).
- ²⁷V. Lattanzi, S. Thorwirth, D. T. Halfen, L. A. Mück, L. M. Ziurys, P. Thaddeus, J. Gauss, and M. C. McCarthy, Angew. Chem., Int. Ed. 49, 5661 (2010).
- ²⁸ K. J. Dykema, T. N. Truong, and M. S. Gordon, J. Am. Chem. Soc. 107, 4535–4541 (1985).
- ²⁹W. Weltner, Magnetic Atoms and Molecules (Scientific and Academic Editions, New York, 1989).
- ³⁰T. D. Varberg, R. W. Field, and A. J. Merer, J. Chem. Phys. 95, 1563 (1991).